Increasing coastal exposure to extreme wave events in the Alaskan Arctic as the open water season expands

Check for updates

Martin Henke [1] ✉, Tyler Miesse[1], André de Souza de Lima[1], Celso M. Ferreira[1] & Thomas M. Ravens[2]

Declining Arctic sea ice over recent decades has been linked to growth in coastal hazards affecting the Alaskan Arctic. In this study, climate model projections of sea ice are utilized in the simulation of an extratropical cyclone to quantify how future changes in seasonal ice coverage could affect coastal waves caused by this extreme event. All future scenarios and decades show an increase in coastal wave heights, demonstrating how an extended season of open water in the Chukchi and Beaufort Seas could expose Alaskan Arctic shorelines to wave hazards resulting from such a storm event for an additional winter month by 2050 and up to three additional months by 2070 depending on climate pathway. Additionally, for the Beaufort coastal region, future scenarios agree that a coastal wave saturation limit is reached during the sea ice minimum, where historically sea ice would provide a degree of protection throughout the year.

Climate change has increasingly been linked to growth in the Arctic Ocean wave climate[1–3]. The primary driver of this growth is the dramatic decline in Arctic sea ice observed in recent decades[4,5] and the consequential increase in ice-free ocean areas. Sea ice limits Arctic wave energy by dissipating incident swells, limiting fetch, and preventing the generation of wind-waves[6–8]. Thus, as sea ice extent continues to retreat, Arctic sea states will be heightened with more wave energy resulting from increased fetch[2,5,9] and longer periods of open water. Consequently, Arctic coastal regions will experience accelerated rates of erosion[10,11], and increased risk of flooding. These trends are projected to continue[12–14] as sea ice decline persists and ice-free summers are expected to occur by mid-century[15].

In the Alaskan Arctic, the increase in wave climate has contributed to growth in coastal hazards[16–19]. These hazards are often associated with extreme weather events such as extratropical cyclones[20], Arctic cyclones[21,22], and strong wind events[21,23,24] which cause high waves and storm surge resulting in coastal inundation and rapid erosion. Historically, most impactful storms occur during the fall season[9,24–26]—when summer open water conditions persist and coincide with the more intense storm events of the fall and early winter seasons[27,28]. As sea ice continues to decline and the expansion of the open water season delays the formation of sea ice in coastal areas to later months[29,30], Arctic shorelines are exposed to a growing number of storm-induced wave hazards[9,31]. This is especially relevant as winter storm intensity equals or surpasses fall intensity[27,32], and extratropical cyclones (typically the most impactful synoptic event causing Alaskan Arctic coastal flooding) trend further northward into the Arctic[27]. This threat is compounded as regional winter month storminess is projected to increase in the coming decades[23,33,34]. Thus, the expanding seasonal window of open water in the Alaskan Arctic threatens to not only expose shorelines to an increased number of storm events, but also to leave shorelines exposed to events of increased intensity. As evidence, recent research hindcasting waves along Alaska's Beaufort shorelines determined that the timing of extreme wave events has trended towards later in the calendar year[35]; however, there is still considerable uncertainty in projecting how future sea ice decline will affect seasonal exposure to coastal hazards impacting Alaskan shorelines. Furthermore, while numerous studies have projected and analyzed the growth in the open-water area and season along Alaskan Arctic coastal and inferred or approximated growing coastal wave heights, robust numerical simulation of coastal wave hazards in conjunction with projected ice fields has yet to be undertaken.

In this study, we assess future sea ice decline within the Alaskan Arctic region and simulate how waves associated with a historical representative storm event would change under future sea ice conditions. Through this framework, the sensitivity of the coastal wave response dependent on regional sea ice extent is established and used to predict future seasonal exposure to wave hazards associated with similar storm events. In contrast to existing wave projections which analyze mean or extreme wave parameters over long temporal scales (seasonal to decadal) and broad spatial scales (pan-Arctic to global), this study analyzes the implications of a respective extreme event using a region-specific high-resolution wave and storm surge model. Given the complexity of physical processes affecting

---

[1]Department of Civil, Environmental, and Infrastructure Engineering, George Mason University, Fairfax, VA, USA. [2]Department of Civil Engineering, University of Alaska Anchorage, Anchorage, AK, USA. ✉e-mail: mhenke@gmu.edu

wave dynamic in coastal areas, the high-resolution physical wave model employed within this study yields more accurate simulations of coastal wave heights (as opposed to alternative methods, such as utilizing off-shore wave heights as proxy or empirical equations) through parameterization of additional dissipative processes. This framework allows insight into the relationship between the regional open-water area and dependent coastal wave response to be identified and compared for varying future periods and emission pathways.

Sea ice analysis

Future sea ice projections analyzed include the SSP2-4.5 and SSP5-8.5 (moderate and high future emissions scenarios, respectively) climate pathways for the decades of 2050–2059 and 2070–2079 (henceforth referred to simply as 2050 and 2070 respectively in conjunction with the specific climate scenario). In this analysis, a multi-model ensemble (MME) was utilized to create a robust projection of future sea ice and to assess trends in regional sea ice extent (SIE).

In comparison to the historical record, both future scenarios show dramatic decreases in pan-Arctic SIE as SSP2-4.5 2050 and 2070 and SSP5-8.5 2050 and 2070 show 71%, 93%, 95%, and 100% reductions in September SIE, respectively (Fig. 1a). The three seasonal curves yielding a greater than 90% September SIE reduction correspond to pan-Arctic SIE below $1 \times 10^6 \, \text{km}^2$, meaning the Arctic is effectively ice-free. When comparing future scenarios with the historical median, it's important to note that in addition to the downward shift in September minimum SIE (potentially increasing the magnitude of coastal hazards), there is a horizontal shift as the open-water season is prolonged, extending the season of exposure to storm-induced coastal hazards. For example, SIE for the SSP5-8.5 2070 curve is below $1 \times 10^6 \, \text{km}^2$ from August to October, thus presenting multiple months of nearly ice-free conditions.

Examination of the SIE within the Alaskan Arctic (within the Alaskan Beaufort and Chukchi Seas, Fig. 1b, c) shows that the projected future fall and winter SIE departs substantially from the historic average and shows that the extent of that departure depends on the climate pathway assumed. The effective upper bound of SIE within this region is $1.77 \times 10^6 \, \text{km}^2$. Beyond this SIE, the sea ice fully covers the region and extends south beyond the Bering Strait. This SIE is assumed to effectively correspond to the complete suppression of waves within the region and is typically reached before December. Contrasting this, median SIE for both scenarios and decades shows the regional maximum SIE not being reached until at least January, with SSP5-8.5 2070 median SIE failing to meet full coverage within the region throughout the year. The historical median September SIE (the seasonal minimum) for the region is plotted at $0.88 \times 10^6 \, \text{km}^2$ and can be interpreted as the SIE which has historically aligned to peak exposure to wave hazards due to maximum seasonal fetch. Future scenarios show dramatic decreases in the seasonal SIE minimum (well below the historic SIE minimum) with all scenarios except for SSP2-4.5 2050 reaching zero sea ice coverage. In both future scenarios, median SIE is below the median historic SIE seasonal minimum until at least November – resulting in a state where open-water area exceeds that of the historical maximum fetch occurring during September for over two months into the autumn.

Extratropical cyclone wave hazards simulation

The storm event analyzed in this research is an extratropical cyclone that impacted Alaska on December 31, 2016. This storm was found to be representative of typical autumn and winter extratropical cyclones which have historically impacted this region[20,27,36-38]. The storm originated within the northern Pacific, progressed along the coast of Siberia, through the Bering Strait, and dissipated within the Chukchi Sea (a commonly occurring extratropical cyclone track correlated with extreme waves and coastal flood events[20,36,38]) as shown in supplementary Fig. S1. This event caused widespread damage to Alaskan coastal communities, as hurricane-force wind gusts caused extensive structural damage in Savoonga, Alaska, generated storm surge, and brought flooding along western and northwestern Alaskan
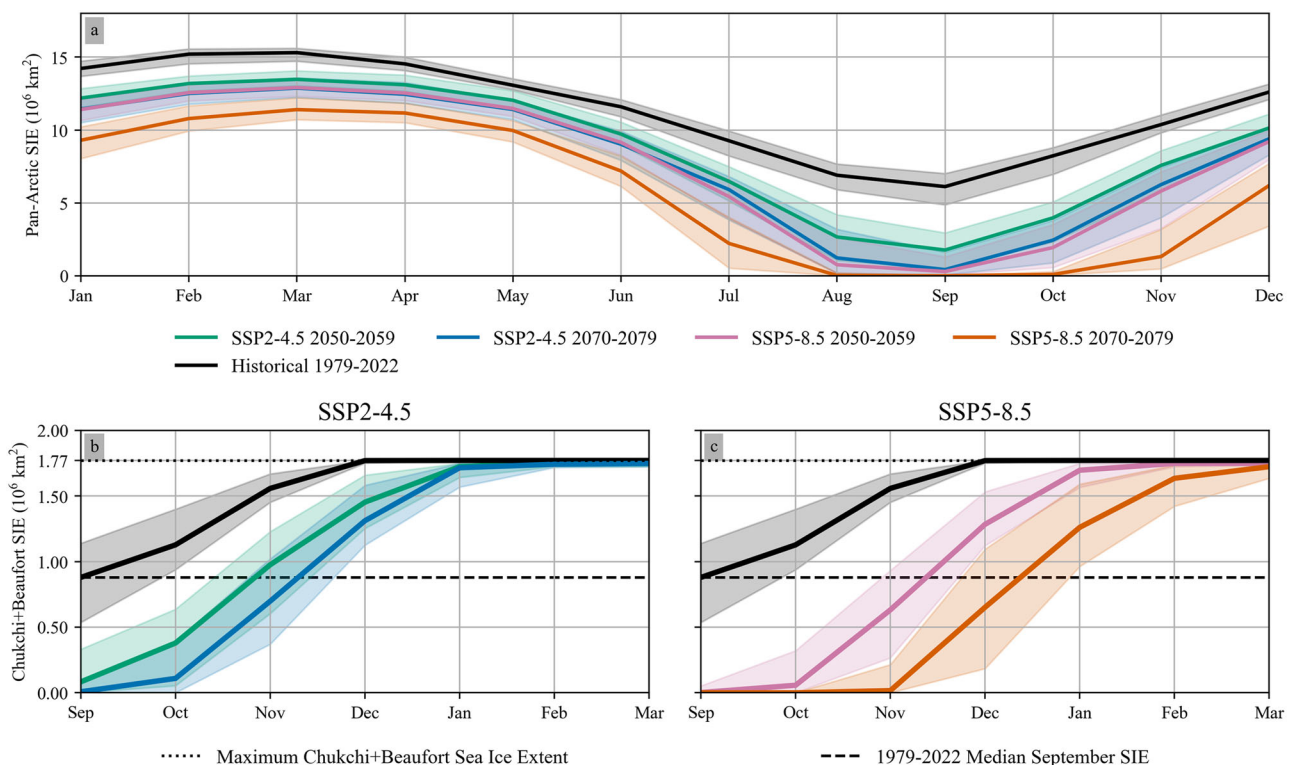

Fig. 1 | **Future scenario sea ice extent curves. a** Pan-Arctic monthly SIE comparison between the SII and MME for the different climate pathways and decades. Chukchi and Beaufort's region combined SIE for (**b**) SSP2-4.5 and (**c**) SSP5-8.5. Shaded regions represent the 2nd and 3rd quartiles in the monthly SIE of either the MME or within the historical record. Dotted and dashed lines indicate the maximum Beaufort+Chukchi SIE and historical seasonal minimum SIE, respectively. Monthly markers denote SIE averaged through the entirety of the respective month.
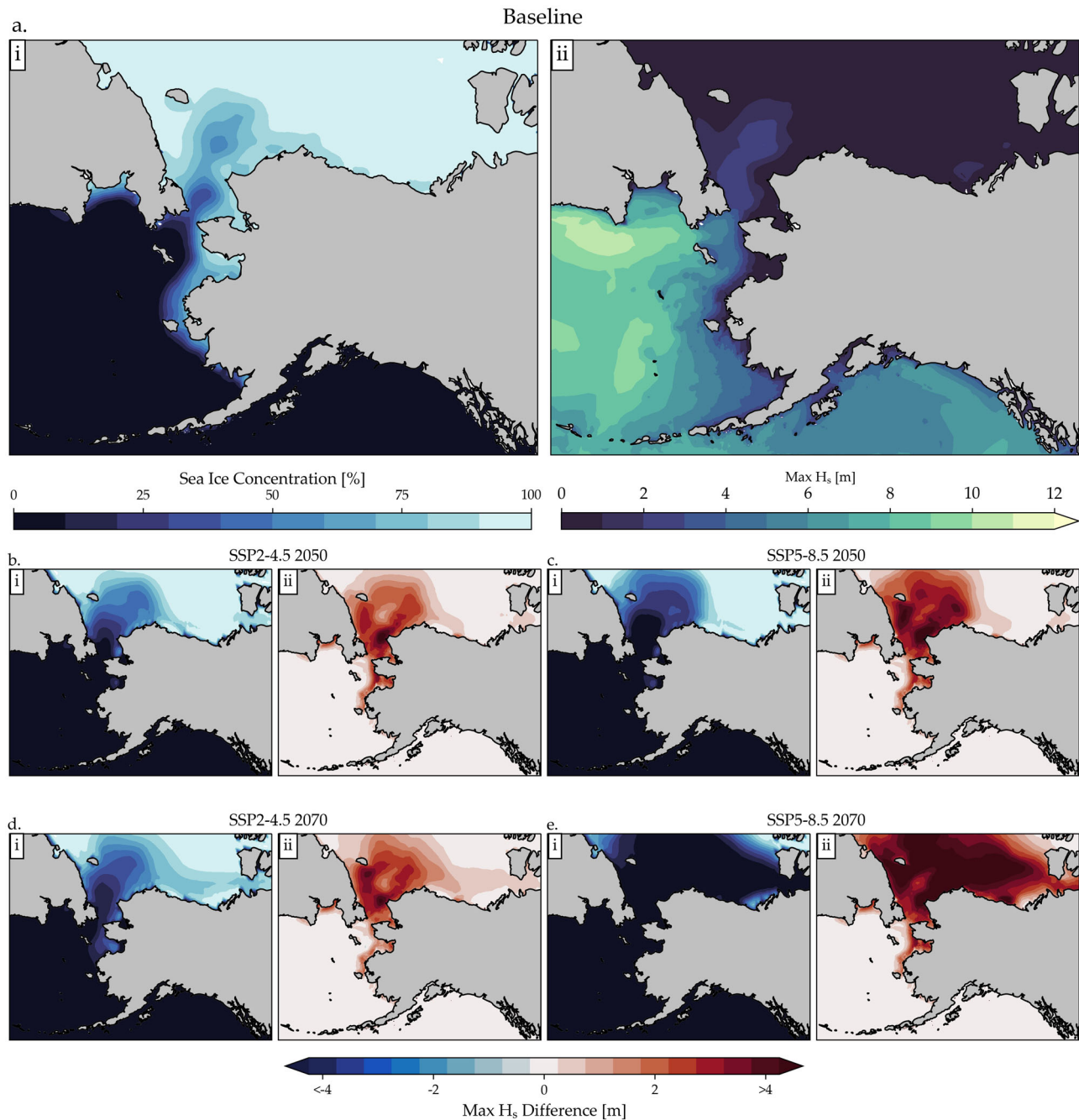
Fig. 2 | Scenario sea ice cover and maximum significant wave height. a Baseline simulation averaged sea ice concentration (left) paired with the maximum significant wave height to occur during simulation (H_{s-max}) (right). Future scenarios' decade simulations shown in (**b**), (**c**), (**d**), and (**e**) display sea ice conentration (left) averged through simulation time and the difference in simulated H_{s-max} (right) relative to the baseline storm simulation. For all future simulation plots, sea ice concentration and H_{s-max} have been averaged among multiple simulation realizations (see Methods for futher description).

shorelines[39–42]. While sea ice extent was unusually low and fragmented at the time[40], newspaper articles reported that sea ice protected coastlines from waves[39].

The employed model simulates waves and water levels on a scale encompassing the entirety of Alaska yet with sufficient resolution to resolve coastal areas (see Methods for further model and input data details). Specifically, wave simulations were produced for the period December 20th through January 9th encompassing the storm event. The historical simulation (henceforth referred to as the baseline simulation) and future simulations differ respectively by using either observed sea ice conditions or climate model projected daily sea ice concentration fields concurrent with the simulation dates yet belonging to a future decade.

Comparing baseline and future scenarios' decade simulations presents a stark contrast, as all future simulations show substantial expansions in the open-water area and resulting growth in the regional sea state. In the baseline simulation (Fig. 2a), the maximum significant wave heights (H_s: the average of the highest third of wave heights) projected to occur during simulation (H_{s-max}) are near-zero for much of the ice-covered Arctic regions north of the Bering Strait – demonstrating how sea ice acted to suppress wave hazards during the storm event. It's worth noting that December 2016 itself possessed anomalously low SIE (below the month's historical 10th percentile) and already represents a reduction from the expected seasonal sea ice protection. In comparison to the baseline, all future simulations (Figs. 2b through 2e) have increased open-water area north of the Bering Strait and subsequently

show substantial growth in $H_{s\text{-}max}$. Thus, the storm had the potential to generate wave hazards further north, yet its impacts along Arctic shorelines were largely mitigated by sea ice present during the storm.

Three of the future simulations: SSP2-4.5: 2050, 2070, and SSP5-8.5 2050, share comparable ice coverage. Due to the projected delay in the expansion of seasonal ice coverage, from December 20th to January 9th, these simulations show that the majority of the Bering Sea is ice-free and that the 75% ice concentration contour lies within the Chukchi Sea. In accordance with this expansion in open-water area, $H_{s\text{-}max}$ grows primarily along western Alaskan coastlines and northward beyond the Bering Strait – with the greatest locale of growth exceeding 4 meters off the northwest point of Alaska. Distinct from other simulations, SSP5-8.5: 2070 (Fig. 2e) projects massive reductions in sea ice coverage, leaving much of the Chukchi and Beaufort Seas almost entirely ice-free. To give context from Fig. 1., SIE for this scenario is lower than the historical median SIE for the month of September—meaning that the available fetch exceeds the fetch during the historical seasonal minimum. This extensive expansion of open water allows for widespread wave growth, as $H_{s\text{-}max}$ rises by over four meters throughout much of the Arctic region and particularly along Alaska's northern coast. Investigation into the timing of $H_{s\text{-}max}$ occurrences within the Beaufort Sea for this simulation reveal many to have occurred at a later date (January 5th – 6th) due to strong westerly winds occurring within the region—a phenomenon known to correlate with coastal hazards along Beaufort shorelines[23] yet was entirely negligible within the baseline simulation due to the presence of sea ice.

Coastal wave heights

Coastal shore segments along the US Chukchi/Bering Sea shorelines (sourced from the Arctic Coastal Dynamics (ACD) database[43]) were used to sample nearshore wave heights. Points falling within the coastal segments (considering model nodes with wave heights greater than 0.5 m; see "Methods" section for details) are used as the basis for the analysis shown in Figs. 3, 4.

Figure 3 shows that in comparison to the baseline simulation shown in Fig. 3a, future scenarios and decades (Fig. 3b through 3e) possess similar increases in the median values of $H_{s\text{-}max}$ on the coastline adjacent to the Chukchi Sea. In the baseline simulation (Fig. 3a), the median $H_{s\text{-}max}$ for

most coastal segments is largely limited to below 0.5 m. However, as sea ice diminishes between future simulations, $H_{s\text{-}max}$ rapidly increases, trending northward along Chukchi shorelines until reaching the minimum SIE simulation in Fig. 3e (SSP5-8.5 2070) which has the maximum wave response, where nearly all Chukchi coastal segments show median $H_{s\text{-}max}$ to exceed 1 m and range up to 3 m. Within the Chukchi region, the most prominent increases in coastal wave heights (common to all future simulations) occur at the northwest tip of Alaska near the community of Point Hope, where median coastal $H_{s\text{-}max}$ ranges from 2 to 3 m during the storm event. Crucially, increases in nearshore wave heights would assumably correspond to a marked increase in coastal hazards associated with the storm event, as waves can increase storm surge through wave radiation stress and further inundation extent through wave runup. Given that coastal flooding was observed for this storm event, which did not produce coastal waves due to nearshore ice, a similar storm occurring when sea ice was reduced would generate relatively large waves (exceeding 1 m) thus enhancing flooding due to wave setup and runup.

The SSP5-8.5 2070 simulation in Fig. 3e is the only one to generate considerable coastal wave activity along Beaufort shorelines. Within the region, barrier island shoreline segments exhibit $H_{s\text{-}max}$ within the range of 1–2 m while the inland shorelines' coastal segments do not exceed 1 m, as these areas are primarily affected by local wind waves. Nonetheless, this result contrasts the near-total suppression of coastal waves seen in baseline and other future simulations and demonstrates the region to be largely unaffected when sea ice loss is limited to the Chukchi Sea. Furthermore, the contrast between this scenario and the alternative emissions pathway (SSP2-4.5) for the same decade in Fig. 3d presents a clear divergence in the outcomes of exposure to coastal hazards. While both show dramatic increases in maximum wave heights for Chukchi coastal areas, the former leaves nearly the entirety of the Beaufort coastal region (hundreds of miles of coastline including large communities such as Utqiaġvik and critical regions of oil and gas development such as Prudhoe Bay) exposed to wave hazards – highlighting how future emissions could drastically alter future exposure.

Future seasonal exposure

To study how simulated storm-induced coastal wave heights vary depending on sea ice coverage, the full ensemble of storm simulations is

Fig. 3 | Coastal wave height segments. Arctic Coastal Dynamics shoreline segments with derived median $H_{s\text{-}max}$ corresponding to each simulation scenario and decade. Results from the baseline simulation are shown in (**a**) while (**b**), (**c**), (**d**), and (**e**) show the future scenarios averaged over realizations before deriving the coastal segment median.
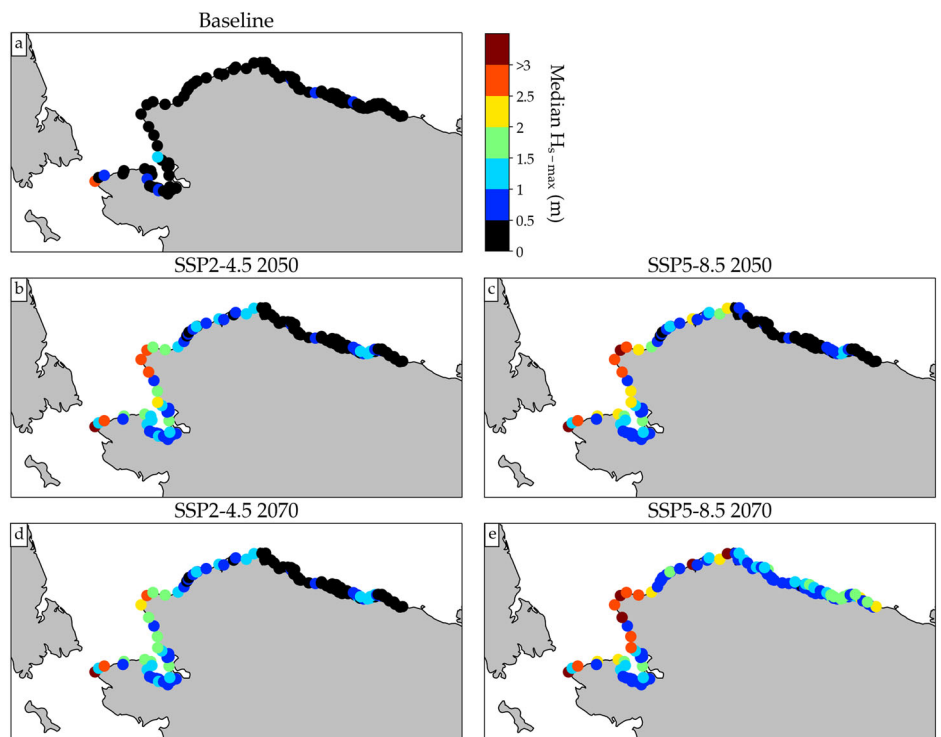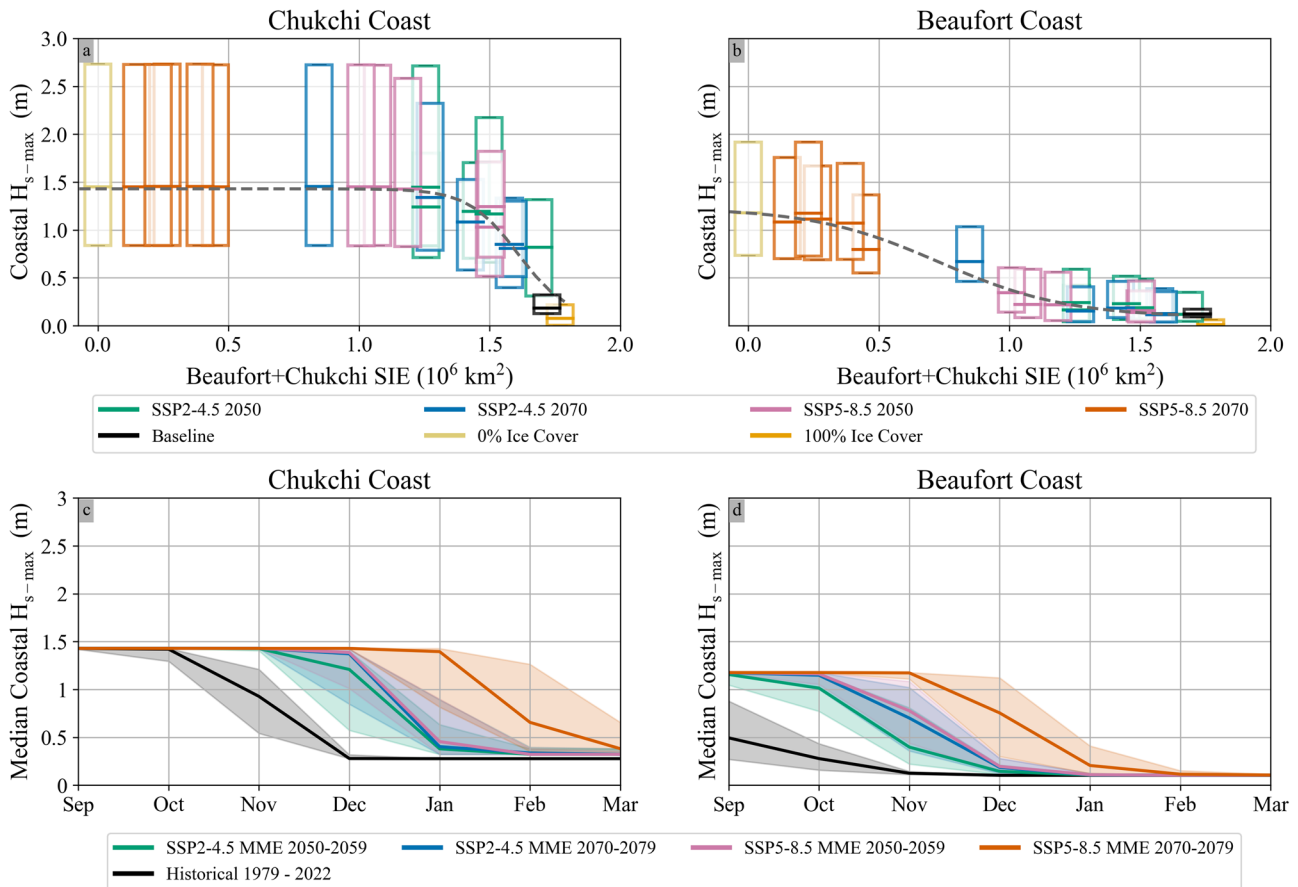
Fig. 4 | Regional coastal wave response and derived seasonal exposure window. Coastal $H_{s\text{-}max}$ values for the Chukchi (**a**) and Beaufort (**b**) coasts as a function of averaged simulation SIE where each boxplot denotes the median and interquartile range in $H_{s\text{-}max}$ with colors denoting the scenario and decade to which each simulation belongs. Additionally, a logistic regression function has been fit to the data and is shown as the black dashed lines, allowing for the maximum saturation and protection thresholds to be observed. Plots (**c**) and (**d**) utilize the derived functions to project the median coastal $H_{s\text{-}max}$ values respective to each region as a function of MME SIE for both regions. Shading indicates the spread derived from the first and third quartile of MME regional SIE.

analyzed. As the simulation ensemble ranges from full ice coverage to entirely open water, the derived relationships between the coastal wave response and sea ice coverage can be related to projected future seasonal monthly sea ice extent. From each simulation, median regional $H_{s\text{-}max}$ values (within the coastal segments using the aforementioned inclusion threshold) were plotted as a function of average SIE during the simulation (Fig. 4). Figure 4 shows that regions possess clear upper and lower thresholds of SIE, beyond which coastal regions reach maximum protection or saturation, respectively. For example, for the Chukchi coastal region (Fig. 4a), the median coastal $H_{s\text{-}max}$ is approximately 0.25 m when the ice cover is maximal (with SIE ~ $1.75 \times 10^6 \text{km}^2$)—representing the threshold of maximum protection. However, as SIE decreases, the median $H_{s\text{-}max}$ rapidly grows and then converges to a saturation limit near 1.5 m at SIE ≈ $1.25 \times 10^6 \text{km}^2$. With only $0.5 \times 10^6 \text{km}^2$ SIE difference between the saturation limit and minimum of coastal wave response, the Chukchi coastal area is shown to be highly sensitive to initial reductions in the combined Chukchi and Beaufort SIE. This result is partially expected as Chukchi sea ice forms after the Beaufort has achieved majority coverage. Interestingly, this region rapidly reaches the saturation limit threshold, beyond which the maximum coastal wave magnitudes do not respond to further reductions in sea ice. Contrasting this observation, Beaufort coastal areas were found to be more resilient to diminishing regional SIE. In the Beaufort, simulations with decreasing SIE resulted in a more gradual response in coastal $H_{s\text{-}max}$, which did not begin to converge to a median saturation limit until the region was entirely ice-free – inferring that wave heights could potentially grow further with further sea ice loss outside the Beaufort Chukchi region.

Utilizing the curve-fits derived in Fig. 4a, b, the more robust MME SIE projections shown in Fig. 1 were used as inputs to project the median coastal $H_{s\text{-}max}$ (respective to this storm) for future months. The resulting seasonal exposure curves shown in Fig. 4c, d allow for future scenarios' extended seasonal duration of open water to be related directly to the potential storm-induced wave response. For the Chukchi coast, near total suppression of waves is typically achieved by December, yet SSP2-4.5 2050, 2070, and SSP5-8.5 2050 do not reach similar levels of protection until a month later in January. SSP5-8.5 2070 never fully reaches the bottom protection threshold and does not come close until March, corresponding to a 3-month extension in seasonal exposure to waves.

For the Beaufort coast, both future scenarios predict an expansion in the seasonal exposure similar to the Chukchi, as the date of expected maximum protection shifts from November to past December. Importantly however, for the Beaufort coast, historical levels of SIE limit coastal wave heights even during the annual sea ice minimum in September. Therefore, future sea ice loss corresponds not only to an expanding window of exposure but also to an increase in coastal wave magnitudes during fall months. This results in future scenarios' median $H_{s\text{-}max}$ value (1.2 m) being over double that of the historical curve's September $H_{s\text{-}max}$ value (0.5 m). In this outcome, both future sea ice scenarios agree in predicting the saturation limit for this storm event will be reached in September and could extend up to November for the SSP5-8.5 scenario in 2070.

Discussion
Both climate pathways analyzed show similar dramatic reductions in SIE by 2050, which corresponds to an extended season of fall and winter coastal

exposure for both the Chukchi and Beaufort coastal zones. Turning to 2070, the two climate pathways diverge as SSP2-4.5 still projects seasonal sea ice coverage comparable to 2050 decadal levels, while SSP5-8.5 projects further sea ice losses setting it far apart from the other climate scenario. Consequently, the derived H_{s-max} projection curves for the latter scenario show a stark increase in the window of coastal wave exposure (Fig. 4c, d) as the time required to reach maximum protection for the Chukchi region is extended by 3 months and the Beaufort region is extended by 2 months relative to the baseline and by at least 1 additional month relative to the other future scenario in 2070. Furthermore, the projection curve in Fig. 4c fails to reach the maximum protection threshold by March, indicating that some level of coastal wave exposure would be present throughout the entire winter. These results show that while there may be little difference between climate pathways in the near future, the SSP5-8.5 scenario of 2070 represents a substantial and potentially disastrous outcome of unmitigated climate change, especially when considering that numerous Alaskan communities are already threatened by previously unprecedented coastal hazards[17,19,44] and there is increasing interest in economic development within the region[45,46].

For this storm event, the Chukchi coast reaches the saturation limit with relatively little SIE loss; demonstrating that the maximum coastal response for this event was primarily dependent on regional Chukchi sea ice coverage rather than increasing open-water areas at higher latitudes or within the Beaufort. Given that fall extratropical cyclones have been some of the most impactful synoptic events causing flooding within the Chukchi coastal region, this finding demonstrates that the magnitude of coastal wave hazards caused by these storms may be limited by other factors other than open-water area – highlighting the complexity of processes affecting regional coastal wave heights and challenging the simplified assumption that increasing available fetch due to reduced sea ice area invariably leads to larger coastal wave heights. Nonetheless, while further increases in the theoretical available fetch may not always directly correspond to increasing wave heights during extreme events, an extended duration of open water leaves coastal regions at exposed to storm events further into the winter. This is a notable outcome considering that winter extratropical cyclones trend further northward and have higher intensity compared to fall cyclones[27]. This shift toward winter seasonal exposure could thereby increase both the incidence of coastal storm hazards and also the magnitude of waves and storm surges.

It should be noted that these results (both upper and lower bounds of H_{s-max} shown in Fig. 4) are derived from the simulation of a single storm under varying ice coverage. One is led to wonder how repeating this experiment with different extratropical storm events would produce shifts in these results. Assumably, the magnitude of H_{s-max} and the observed saturation limits would change for storms of varying intensity and tracks. Nonetheless, the December 2016 extratropical cyclone event simulated for this study followed an identifiable track common to the extratropical cyclones which routinely impact the Chukchi region[27,37] and is thus taken as a representative event. However, despite the acknowledged routine nature of these cyclones and considerable damage caused, there is a distinct lack of assessment of the regional spatiotemporal patterns of wave hazards and storm surge characteristic to these events. As coastal modeling capabilities are being developed throughout the region, assessment of storm climatology, providing information on common tracks, intensity variability, and seasonality would provide crucial knowledge.

In addition, other types of synoptic events such as Arctic cyclones, anticyclones, and extreme wind events can cause substantial coastal hazards along Alaskan Arctic shorelines. As with extratropical cyclones, there is little research into characterizing the spatiotemporal patterns of coastal hazards caused by these other Arctic extreme weather events. This is understandable, given that Arctic cyclones are most prevalent and intense during the winter[22,47] when extensive sea ice is present and thus both storm surge and waves are limited. This was observed within this study, where H_{s-max} values for the Beaufort coastlines occurred at a later date (January 5th) from the extratropical cyclone and were caused by high westerly winds adjacent to the

Beaufort coast – a wind event that generated no discernable waves in the baseline simulation, but substantial waves in SSP5-8.5 2070 simulations. In this regard, it's clear that the spatial distribution and seasonality of sea ice would affect the coastal wave response for these events differently, and thus specific investigation is required within future studies. As another consideration, future changes in storm climatology may also affect the seasonality and magnitude of coastal storm hazards for the Alaskan Arctic as increasing open-water area results in greater cyclogenesis and wind speeds[48,49]. While there is still considerable uncertainty in future trends of cyclone activity within the circumpolar Arctic[50]; within the Alaskan Arctic, there has been evidence of increased regional storminess, increasing Arctic cyclone activity, and a poleward shift in extratropical cyclones[23,32,33,50–52]. However, specifically for extratropical cyclones, these projected changes have not been shown to represent a substantial deviation from the historic seasonal climatology and thus the use of the historic storm used within this simulations is assumed acceptable in future scenario simulations. Nonetheless, future assessment utilizing projected trends in extratropical cyclones entering the Alaskan Arctic and shifts in Arctic cyclone climatology is necessary for robust prediction of future coastal hazards frequency and magnitude affecting the region.

Finally, in assessing Arctic coastal wave exposure, accounting for the presence of coastal landfast sea ice persisting beyond the expansion of the sea ice edge reaching the coast is an important consideration. Recent research from Hosekova et al.[53] has demonstrated that without accounting for the presence of landfast ice, seasonal estimations of open water wave exposure along Alaskan Arctic coastlines could be greatly overestimated through the spring and early summer seasons. Taking this into consideration with the fact that projections of landfast sea ice formation and break-up do not currently exist, this study chose to limit analysis of the expansion of open water into the fall and winter season. This decision was deemed acceptable considering that autumn landfast sea ice typically does not greatly precede the arrival of the Arctic sea ice edge, thus reducing our error in projecting coastal wave exposure during this season[53,54]. Furthermore, in comparison to spring, autumn landfast sea ice is more fragmented and is much less capable of protecting coastal areas; where the landfast sea ice itself can be destabilized, detached, and compound with other extreme event coastal hazards – a phenomenon observed for the December 2016 storm study analyzed within this study[40]. Nonetheless, the inability to project the timing of landfast sea ice formation along the coast does incur a degree of uncertainty in the results and remains an unanswered question under future climate changes scenarios.

Methods
Sea ice projections
To project trends in declining sea ice, a multi-model ensemble (MME) was formed of global climate models (GCM) selected from the Coupled Model Intercomparison Project's sixth phase (CMIP6)[55]. The MME was created for two shared socioeconomic pathways, namely SSP2-4.5 and SSP5-8.5 (moderate and high future emissions scenarios, respectively), and consists of 14 and 15 models, respectively. Models included within the MME were selected based on previous research assessing accuracy in predicting SIA during the month of September for the historic period[15]. A maximum contribution of 5 realizations was taken for each model depending on the number available. A comprehensive description of the MME including the specific models and the number of realizations can be found within the Supplementary Table 1. For both climate pathways, two decades were sampled, 2050 and 2070, and monthly sea ice extent (SIE) was determined. SIE is the sum of area for all model cells exceeding 15% sea ice concentration. Historic SIE was extracted from the National Snow and Ice Data Center's (NSIDC) Sea Ice Index[56]. Regional analysis of the combined Chukchi and Beaufort Seas SIE was delineated in accordance to the NSIDC definition of each region[57] shown in Supplementary Fig. S1. To insure even weighting between all ensemble members in calculating MME SIE, the mean of all realizations belonging to individual models taken first before averaging between climate models. From the MME, a single model (CESM2-

WACCM) was used to provide sea ice fields for use in the storm simulation. Sea ice was sourced from the middle of the selected decades (2055 and 2075) with 5 ensemble members available for both climate scenarios SSP5-8.5 and 2-4.5.

Storm simulation

The ADCIRC + SWAN (ADvanced CIRCulation + Simulating WAves Nearshore) coupled model is used for numerical simulations of astronomical tides, storm surge[58,59], and waves[60] as a function of forcing fields: wind, pressure, and sea ice concentration. Individually, both models have been used within the Alaska region to simulate water levels[61,62] and waves[35,63,64]. Through recent model developments, existing sea ice parameterizations for both storm surge[61] and wave dissipation[8] have been implemented into the coupled model. In ADCIRC, the effect of sea ice on tides and surge is modeled through newly implemented parameterization developed by Joyce et al.[61]. This implementation has been shown to represent the effect of sea ice amplifying storm surge under partial sea ice coverage while suppressing surge under high sea ice coverage[65]. Within SWAN, wave dissipation through ice fields is represented by the parameterization commonly known as IC4M2[66] which has recently been added into the model[8]. This parameterization has been utilized within Alaska and has shown reasonable performance in modeling wave attenuation by sea ice under a variety of scales, seasons, and sea ice conditions[35,63]. For this simulation, accounting for the expansive domain and assumed variety of sea ice conditions, we default to utilizing the coefficients derived by Meylan et al.[66] for use with IC4M2.

A previous study utilizing this model (without sea ice parameterizations) with identical mesh, validated the model and showed it to possess reasonable accuracy in simulating storm water levels and waves during the summer season[62]. Additionally, validation of waves was performed in reference to the ESA Remote Sensing Significant Wave Height L3 product[67] over the period December 25th, 2016 to January 5th 2017. Plots showing locations of satellite validation points and model correlation can be seen in Supplementary Fig. S2 and the model correlation coefficient was determined to be 0.97 with mean bias of -0.42 m. From these metrics, we believe the model's performance to be acceptable and furthermore assume that any bias present within the model will persist between experiment simulations. In order to provide additional validation specific to the Chukchi and Beaufort Coastal Regions, an additional validation simulation was performed for August 2019 while multiple near-shore wave buoys were concurrently in operation. From this validation, Fig. S3 shows that mean bias does not exceed 10 cm for any of the stations and the correlation coefficient exceeds 0.85 for all buoys. This validation demonstrates the mode possesses reasonable accuracy in near-shore wave simulation over the wide coastal area encompassed by the model domain.

To create the storm simulation ensemble, a total of 23 simulations were performed for varying sea ice fields representing either historically observed, climate model projected, fully ice-free, or entirely ice-covered conditions. All simulations of the December 2016 storm were run for 21 days ranging from December 20th to January 9th and utilize hourly meteorology (10 m wind velocity and mean sea level pressure) forcing fields sourced from the European Center for Medium-Range Weather Forecasts' ERA5[68] climate reanalysis. For the baseline simulation, sea ice data was also obtained from ERA5 while for future decades the projected sea ice fields were sourced from the CESM2-WACCM model and linearly interpolated onto the ERA5 grid. There are 5 available ensemble members for each future climate scenario and thus a single storm simulation is performed using daily sea ice specific to the year, emissions pathway, and ensemble member – making for a total of 20 simulations performed using climate model projected sea ice fields. Finally, two additional simulations were performed to establish an upper and lower bound of sea ice coverage. An ice-free simulation, without sea ice as an input, and an ice-full simulation, where all sea ice input grid points within the Beaufort and Chukchi Seas are given a sea ice concentration of 100%.

Analysis

Storm simulation results are averaged among realizations to account for internal variability within the climate model and the resulting averaged sea ice and $H_{s\text{-}max}$ wave fields are shown in Fig. 2. Here it should be noted that because sea ice fields are averaged over time and ensemble members, there are large artifact areas of marginal ice coverage, where the ice edge for individual ensemble members is more distinct.

For coastal wave analysis, the Arctic Coastal Dynamics (ACD) database[43] was used to assess wave heights along specified US Chukchi/Bering Sea shoreline segments. A number of segments such as sheltered deltas or lagoons with minimal wave action were excluded from analysis, resulting in 106 shore segments used to sample nearshore wave heights. To focus analysis on locations where impactful waves would have occurred if not for the presence of sea ice, a threshold was set for point inclusion where only model nodes that achieve $H_{s\text{-}max}$ values exceeding 0.5 m during an ice-free simulation are sampled in deriving Figs. 3 and 4. The coastal segment names, locations, original number of mesh nodes contained, number of nodes excluded by the threshold, and the median of $H_{s\text{-}max}$ values within the segment can be found in Supplementary Table S2.

Data availability

The climate model data used for simulations and the multi-model ensemble is freely available from the World Climate Research Programme at: https://esgf-node.llnl.gov/projects/cmip6/. ERA5 surface wind speed used in storm simulations be accessed through the climate data store available at https://cds.climate.copernicus.eu/. Wave model validation was done in comparison to the ESA Remote Sensing Significant Wave Height L3 product openly available at https://archive.ceda.ac.uk/, and in comparison to the wave buoy data made available through the Alaska Ocean Observing System accessible at https://aoos.org/. The simulated Hs-max data for baseline and future climate scenario storm simulations are available through https://doi.org/10.4211/hs.9ae612af600c4325a809b010107d5ae9.

References

1. Stopa, J. E., Ardhuin, F. & Girard-Ardhuin, F. Wave climate in the Arctic 1992-2014: Seasonality and trends. *Cryosphere* **10**, 1605–1629 (2016).
2. Thomson, J. & Rogers, W. E. Swell and sea in the emerging Arctic Ocean. *Geophys. Res. Lett.* **41**, 3136–3140 (2014).
3. Liu, Q., Babanin, A. V., Zieger, S., Young, I. R. & Guan, C. Wind and wave climate in the Arctic Ocean as observed by altimeters. *J. Clim.* **29**, 7957–7975 (2016).
4. Thomson, J. et al. Emerging trends in the sea state of the Beaufort and Chukchi seas. *Ocean Model.* **105**, 1–12 (2016).
5. Waseda, T. et al. Correlated increase of high ocean waves and winds in the ice-free waters of the Arctic Ocean. *Sci. Rep.* **8**, 1–9 (2018).
6. Squire, V. A. Ocean Wave Interactions with Sea Ice: A Reappraisal. *Annu. Rev. Fluid Mech.* **52**, 37–60 (2020).
7. Collins, C. O., Rogers, W. E. & Lund, B. An investigation into the dispersion of ocean surface waves in sea ice. *Ocean Dyn.* **67**, 263–280 (2017).
8. Rogers, W. E. Implementation of Sea Ice in the Wave Model SWAN. *Naval Research Laboratory*. **19**-9874, 1–25 (2019).
9. Barnhart, K. R., Overeem, I. & Anderson, R. S. The effect of changing sea ice on the physical vulnerability of Arctic coasts. *Cryosphere* **8**, 1777–1799 (2014).
10. Irrgang, A. M. et al. Drivers, dynamics and impacts of changing Arctic coasts. *Nat. Rev. Earth Environ.* **3**, 39–54 (2022).
11. Nielsen, D. M. et al. Increase in Arctic coastal erosion and its sensitivity to warming in the twenty-first century. *Nat. Clim. Change* **12**, 263–270 (2022).

12. Casas-Prat, M. & Wang, X. L. Sea ice retreat contributes to projected increases in extreme arctic ocean surface waves. *Geophys. Res. Lett.* **47**, 1–11 (2020).

13. Casas-Prat, M. & Wang, X. L. Projections of extreme ocean waves in the arctic and potential implications for coastal inundation and erosion. *J. Geophys. Res.: Oceans* **125**, 1–18 (2020).

14. Khon, V. C. et al. Wave heights in the 21 st century Arctic Ocean simulated with a regional climate model. *Geophys. Res. Lett.* **41**, 2956–2961 (2014).

15. Docquier, D. & Koenigk, T. Observation-based selection of climate models projects Arctic ice-free summers around 2035. *Commun. Earth Environ.* **2**, 1–8 (2021).

16. Williams, D. M. & Erikson, L. H. Knowledge Gaps Update to the 2019 IPCC Special Report on the Ocean and Cryosphere: Prospects to Refine Coastal Flood Hazard Assessments and Adaptation Strategies With At-Risk Communities of Alaska. *Front. Clim.* **3**, 1–11 (2021).

17. Buzard, R. M., Turner, M. M., Miller, K. Y., Antrobus, D. C. & Overbeck, J. R. Erosion Exposure Assessment of Infrastructure in Alaska Coastal Communities. https://doi.org/10.14509/30672 (2021).

18. Overbeck, J. R., Buzard, R. M., Turner, M. M., Miller, K. Y. & Glenn, R. J. T. Shoreline Change at Alaska Coastal Communities. https://doi.org/10.14509/30552 (2020).

19. Buzard, M., Overbeck,. J. R., Chriest, J., Endres, K. & Plumb, E. Coastal flood impact assessments for Alaska communities. *Alaska Div. Geol. Geophys. Survey Rep.* **2021**-1, 1–26 (2021).

20. Wicks, A. J. & Atkinson, D. E. Identification and classification of storm surge events at Red Dog Dock, Alaska, 2004–2014. *Natl. Hazards* **86**, 877–900 (2017).

21. Cassano, E. N., Lynch, A. H., Cassano, J. J. & Koslow, M. R. Classification of synoptic patterns in the western Arctic associated with extreme events at Barrow, Alaska, USA. *Clim. Res.* **30**, 83–97 (2006).

22. Rinke, A. et al. Extreme cyclone events in the Arctic: Wintertime variability and trends. *Environ. Res. Lett.* **12**, 1–11 (2017).

23. Bieniek, P. A., Erikson, L. & Kasper, J. Atmospheric circulation drivers of extreme high water level events at foggy Island Bay, Alaska. *Atmosphere* **13**, 1–17 (2022).

24. Lynch, A. H., Curry, J. A., Brunner, R. D. & Maslanik, J. A. Toward an integrated assessment of the impacts of extreme wind events on Barrow, Alaska. *Bull. Am. Meteorol. Soc.* **85**, 209–221 (2004).

25. Lynch, A. H., Lestak, L. R., Uotila, P., Cassano, E. N. & Xie, L. A factorial analysis of storm surge flooding in Barrow, Alaska. *Mon. Weather Rev.* **136**, 898–912 (2008).

26. Fang, Z., Freeman, P. T., Field, C. B. & Mach, K. J. Reduced sea ice protection period increases storm exposure in Kivalina, Alaska. *Arctic Sci.* **4**, 525–537 (2018).

27. Mesquita, M. D. S., Atkinson, D. E. & Hodges, K. I. Characteristics and variability of storm tracks in the North Pacific, Bering Sea, and Alaska. *J. Clim.* **23**, 294–311 (2010).

28. Atkinson, D. E. Observed storminess patterns and trends in the circum-Arctic coastal regime. *Geo-Marine Lett.* **25**, 98–109 (2005).

29. Barnhart, K. R., Miller, C. R., Overeem, I. & Kay, J. E. Mapping the future expansion of Arctic open water. *Nat. Clim. Change* **6**, 280–285 (2016).

30. Crawford, A., Stroeve, J., Smith, A. & Jahn, A. Arctic open-water periods are projected to lengthen dramatically by 2100. *Commun. Earth Environ.* **2**, 1–10 (2021).

31. Overeem, I. et al. Sea ice loss enhances wave action at the Arctic coast. *Geophys. Res. Lett.* **38**, 1–6 (2011).

32. Redilla, K., Pearl, S. T., Bieniek, P. A. & Walsh, J. E. Wind climatology for Alaska: Historical and future. *Atmos. Clim. Sci.* **09**, 683–702 (2019).

33. Sepp, M. & Jaagus, J. Changes in the activity and tracks of Arctic cyclones. *Climatic Change* **105**, 577–595 (2011).

34. Basu, S. & Walsh, J. E. Climatological characteristics of historical and future high-wind events in Alaska. *Atmos. Clim. Sci.* **08**, 373–394 (2018).

35. Nederhoff, K., Erikson, L., Engelstad, A., Bieniek, P. & Kasper, J. The effect of changing sea ice on wave climate trends along Alaska's central Beaufort Sea coast. *Cryosphere* **16**, 1609–1629 (2022).

36. Francis, O. P. & Atkinson, D. E. Synoptic forcing of wave states in the southeast Chukchi Sea, Alaska, at an offshore location. *Natl. Hazards* **62**, 1169–1189 (2012).

37. Pingree-Shippee, K. A., Shippee, N. J. & Atkinson, D. E. Overview of Bering and Chukchi Sea wave states for four severe storms following common synoptic tracks. *J. Atmos. Oceanic Technol.* **33**, 283–302 (2016).

38. Mesquita, M. D. S., Atkinson, D. E., Simmonds, I., Keay, K. & Gottschatck, J. New perspectives on the synoptic development of the severe October 1992 Nome storm. *Geophys. Res. Lett.* **36**, 1–5 (2009).

39. Demer, L. Winter storm in Savoonga draws experts in weather, emergencies. *Anchorage Daily News* https://www.adn.com/alaska-news/2017/01/05/winter-storm-in-savoonga-draws-experts-in-weather-emergencies/ (2017).

40. Bogardus, R. et al. Mid-Winter Breakout of Landfast Sea Ice and Major Storm Leads to Significant Ice Push Event Along Chukchi Sea Coastline. **8**, 1–18 (2020).

41. Oliver, S. G. Winter storm slams western Alaska coast. *Arctic Sounder* http://www.thearcticsounder.com/article/1701winter_storm_slams_western_alaska_coast (2017).

42. National Climatic Data Center, NESDIS, NOAA & U.S. Department of Commerce. NCDC Storm Events Database.

43. Lantuit, H. et al. The arctic coastal dynamics database: A new classification scheme and statistics on arctic permafrost coastlines. *Estuaries Coasts* **35**, 383–400 (2012).

44. University of Alaska Fairbanks Institute of Northern Engineering, U.S. Army Corps of Engineers Alaska District, U.S U.S. Army Corps of Engineers Cold Regions Research and Engineering & Laboratory. *Statewide Threat Assessment: Identification of Threats from Erosion, Flooding, and Thawing Permafrost in Remote Alaska Communities*. (2019).

45. Aksenov, Y. et al. On the future navigability of Arctic sea routes: High-resolution projections of the Arctic Ocean and sea ice. *Marine Policy* **75**, 300–317 (2017).

46. Mudryk, L. R. et al. Impact of 1, 2 and 4 °C of global warming on ship navigation in the Canadian Arctic. *Nat. Clim. Change* **11**, 673–679 (2021).

47. Zhang, X., Walsh, J. E., Zhang, J., Bhatt, U. S. & Ikeda, M. Climatology and interannual variability of Arctic cyclone activity: 1948–2002. *J. Clim.* **17**, 2300–2317 (2004).

48. Mioduszewski, J., Vavrus, S. & Wang, M. Diminishing Arctic sea ice promotes stronger surface winds. *J. Clim.* **31**, 8101–8119 (2018).

49. Vihma, T. Effects of arctic sea ice decline on weather and climate: A review. *Surv. Geophys.* **35**, 1174–1214 (2014).

50. Walsh, J. E. et al. Extreme weather and climate events in northern areas: A review. *Earth-Sci. Rev.* **209**, 103324 (2020).

51. Yin, J. H. A consistent poleward shift of the storm tracks in simulations of 21st century climate. *Geophys. Res. Lett.* **32**, 1–4 (2005).

52. Michaelis, A. C. & Lackmann, G. M. Climatological changes in the extratropical transition of tropical cyclones in high-resolution global simulations. *J. Clim.* **32**, 8733–8753 (2019).

53. Hošeková, L. et al. Landfast ice and coastal wave exposure in Northern Alaska. *Geophys. Res. Lett.* **48**, 1–11 (2021).

54. Mahoney, A. R., Eicken, H., Gaylord, A. G. & Gens, R. Landfast sea ice extent in the Chukchi and Beaufort Seas: The annual cycle and decadal variability. *Cold Regions Sci. Technol.* **103**, 41–56 (2014).

55. SIMIP Community. Arctic Sea Ice in CMIP6. *Geophys. Res. Lett.* **47**, 1–11 (2020).

56. Fetterer, F., Knowles, K., Meier, W. N., Savoie, M. & Windnagel, A. K. Sea Ice Index, Version 3. https://doi.org/10.7265/N5K072F8 (2017).
57. Meier, W. N. & Stewart, J. S. Arctic and antarctic regional masks for sea ice and related data products, Version 1. https://doi.org/10.5067/CYW3O8ZUNIWC (2023).
58. Westerink, J. J., Luettich, R. A. & Muccino, J. C. Modelling tides in the western North Atlantic using unstructured graded grids. *Tellus A* **46**, 178–199 (1994).
59. Resio, D. T. & Westerink, J. J. Modeling the physics of storm surges. *Phys. Today* **61**, 33–38 (2008).
60. Dietrich, J. C. et al. Modeling hurricane waves and storm surge using integrally-coupled, scalable computations. *Coastal Eng.* **58**, 45–65 (2011).
61. Joyce, B. R. et al. High resolution modeling of western Alaskan tides and storm surge under varying sea ice conditions. *Ocean Model.* **141**, 101421 (2019).
62. Cassalho, F. et al. Intercomparing atmospheric reanalysis products for hydrodynamic and wave modeling of extreme events during the open-water Arctic season. *Arctic Antarctic Alpine Res.* **54**, 125–146 (2022).
63. Branch, R. et al. Modeling sea ice effects for wave energy resource assessments. *Energies* **14**, 1–15 (2021).
64. Hošeková, L., Malila, M. P., Rogers, W. E. & Roach, L. A. Attenuation of ocean surface waves in pancake and frazil sea ice along the coast of the Chukchi Sea *J. Geophys. Res.: Oceans*. (2020) https://doi.org/10.1029/2020JC016746.
65. Kim, J., Murphy, E., Nistor, I., Ferguson, S. & Provan, M. Numerical analysis of storm surges on Canada's western arctic coastline. *J. Marine Sci. Eng.* **9**, 1–20 (2021).
66. Meylan, M. H., Bennetts, L. G. & Kohout, A. L. In situ measurements and analysis of ocean waves in the Antarctic marginal ice zone. *Geophys. Res. Lett.* **41**, 5046–5051 (2014).
67. Piollé, J.-F., Dodet, G. & Quilfen, Y. ESA Sea State Climate Change Initiative (Sea_State_cci): Global remote sensing daily merged multi-mission along-track significant wave height from altimetry, L3 product, version 3. https://doi.org/10.5285/e6af67fca81c40b7bb3eddaadde06909 (2022).
68. Hersbach, H. et al. The ERA5 global reanalysis. 1–51 (2020) https://doi.org/10.1002/qj.3803.

Author contributions
M.H. conceptualized the research, performed analysis, and wrote the manuscript. T.M. and A.S.L assisted in analysis. C.F. and T.R. advised on methodology the discussion of results. All authors reviewed the manuscript.

Competing interests
The authors declare no competing interests.

Additional information
Supplementary information The online version contains supplementary material available at https://doi.org/10.1038/s43247-024-01323-9.

Correspondence and requests for materials should be addressed to Martin Henke.

Peer review information *Communications Earth & Environment* thanks the anonymous reviewers for their contribution to the peer review of this work. Primary Handling Editors: Nicole Khan, Heike Langenberg. A peer review file is available.

Reprints and permissions information is available at http://www.nature.com/reprints

Publisher's note Springer Nature remains neutral with regard to jurisdictional claims in published maps and institutional affiliations.